ChemBioChem

Research Article
doi.org/10.1002/cbic.202500578

Chemistry Europe
European Chemical Societies Publishing

www.chembiochem.org

# Interactions of Neurodegenerative Disease Positron Emission Tomography Imaging Probe Candidates with the C-Terminus of α-Synuclein Fibrils

Kyle D. Shaffer, Ryann M. Perez, Marshall G. Lougee, Vinayak V. Pagar, Hee Jong Kim, Ho Young Kim, Benjamin A. Garcia, Robert H. Mach, and E. James Petersson*

Fibrillar aggregation of α-synuclein (αS) is a hallmark of Parkinson's disease (PD) and related disorders, including multiple system atrophy (MSA) and dementia with Lewy bodies (DLB). Herein, the fibril interactions of two candidate positron emission tomography (PET) imaging ligands, M503 and HY-215, being developed for imaging of PD/DLB and MSA, respectively, are investigated. Photo-crosslinking mass spectrometry is used to determine the sites of their binding to in vitro fibrils, and Förster resonance energy transfer with fluorescently labeled proteins is used to analyze conformational changes in the disordered αS C-terminus. Taken together, these studies show that the MSA-selective PET lead, HY-215, interacts with the C-terminus, unlike the PD-selective lead M503. This study indicates that interactions with the often-ignored disordered regions of αS fibrils should be considered in the development of PET probes and other therapeutic small molecules.

## 1. Introduction

Alpha-synuclein (αS) is an intrinsically disordered protein known to form fibrillar intracellular aggregates that are associated with the pathology of several neurodegenerative disorders, termed synucleinopathies, including Parkinson's disease (PD), dementia with Lewy bodies (DLB), and multiple system atrophy (MSA).[1] Although these diseases all feature αS aggregation, they vary in their clinical and biochemical characteristics. Additionally, MSA is known to have two subtypes: cerebellar ataxia–predominant (MSA-C) and parkinsonism-predominant (MSA-P), characterized by increased copathology of amyloid beta (Aβ) and tau, respectively.[2] Cryogenic electron microscopy (cryo-EM) and solid-state nuclear magnetic resonance (ssNMR) studies have shown that αS can adopt a number of different polymorphs in these fibrillar aggregates.[3–6] The differences in these polymorphs may be partially attributed to differences in physiopathology between diseases. Fibrillar αS in PD/DLB accumulates as insoluble inclusions in neurons, known as Lewy bodies, whereas in MSA, the fibrils accumulate in glial cells, forming glial cytoplasmic inclusions.[7] A variety of polymorphs have been observed for in vitro αS preparations, and there are significant differences in the polymorphs seen in cryo-EM and ssNMR studies of fibrils purified or amplified from PD/DLB patients and those from MSA patients (**Figure 1**).[3,4,8] These structural differences are undoubtedly related to the different pathological characteristics of PD and MSA, and they provide an opportunity to develop molecular tools for tracking the progression of the diseases.

Advancements in the study of Alzheimer's disease have employed positron emission tomography (PET) as a noninvasive method of imaging and quantifying aggregates of tau and Aβ.[9] Using small molecule PET tracers that bind specifically to tau or Aβ fibrils allows for early detection and monitoring of changes in fibril burden during disease progression and treatment. For PD and MSA, no such compounds have been approved for clinical use to date, but several αS PET radiotracers are under development.[10] These include the early lead compound BF-2846, and derivatives M503 and HY-215, which have advanced to human trials for imaging of PD and MSA, respectively (Figure 1).[11,12] In order to optimize the affinity and selectivity of αS PET probe candidates, we and others have worked to obtain structural information on their interactions with fibrils through direct methods like cryo-EM and ssNMR, as well as indirect methods like photo-crosslinking and fluorescence studies.[12–17] While cryo-EM and ssNMR can provide high resolution data on binding in the well-folded fibril core (typically composed of residues 35–100), the molecular interactions and conformational dynamics of the disordered N- and C-termini are critically unresolved for these

*K. D. Shaffer, R. M. Perez, M. G. Lougee, V. V. Pagar, E. J. Petersson*
*Department of Chemistry*
*University of Pennsylvania*
*231 S. 34th Street, Philadelphia, PA 19104, USA*
*E-mail: ejpetersson@sas.upenn.edu*

*H. J. Kim, B. A. Garcia*
*Department of Biochemistry and Biophysics*
*University of Pennsylvania*
*3620 Hamilton Walk, Philadelphia, PA 19104, USA*

*H. Y. Kim, R. H. Mach*
*Department of Radiology*
*University of Pennsylvania*
*3400 Spruce Street, Philadelphia, PA 19104, USA*

*Supporting information for this article is available on the WWW under https://doi.org/10.1002/cbic.202500578*

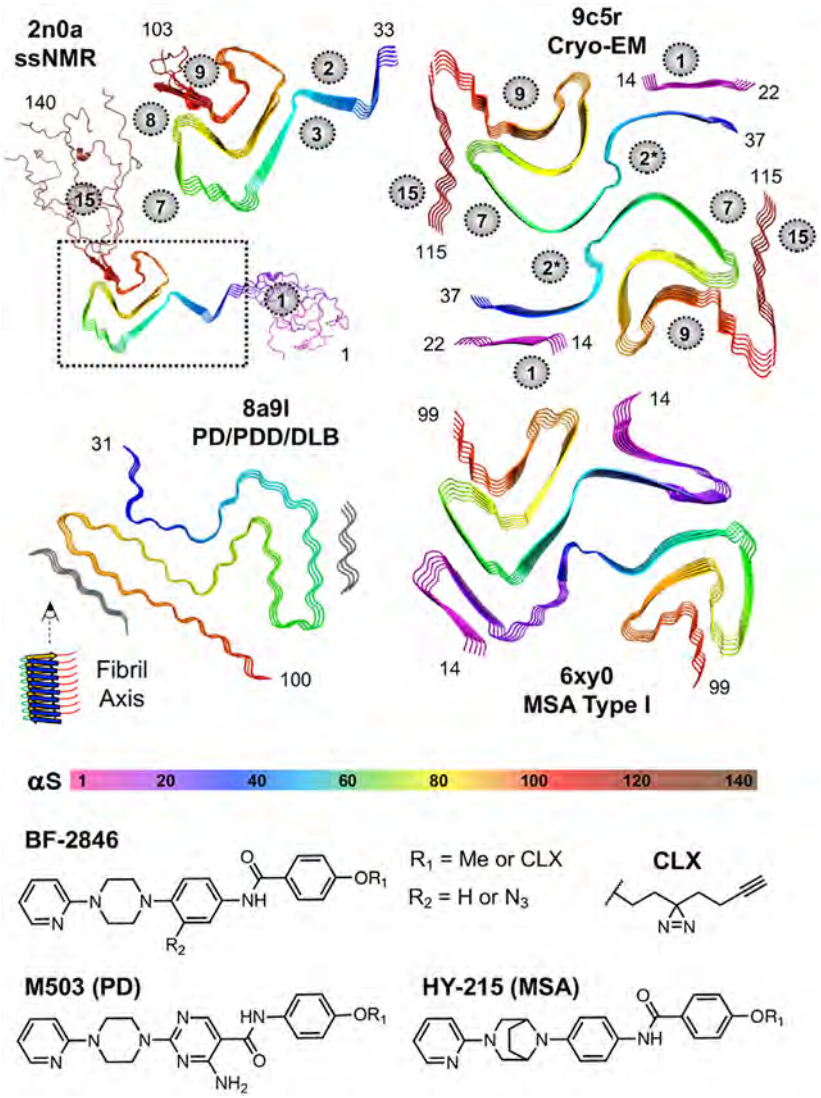


**Figure 1.** αS fibril and ligand structures. Top: In vitro ssNMR or cryo-EM fibril structures and ex vivo PD/PDD/DLB or MSA fibril structures rendered from noted PDB ID coordinates and colored according to the rainbow scheme below the structures.[3,4,8,36] Binding sites identified in computational analysis of PDB ID 2n0a are noted with gray circles.[33] Bottom: Candidate PET ligand structures and crosslinkable analogs used in XL-MS.

methods. However, low resolution models of disordered regions can be constructed from Förster resonance energy transfer (FRET) measurements to provide valuable insight into interactions that can influence polymorph selectivity.[18]

FRET is a powerful tool for probing protein structure and dynamics, taking advantage of nonradiative energy transfer resulting from resonance interactions of the electronic transition dipoles of chromophores.[19] The efficiency of this energy transfer ($E_{FRET}$) is very sensitive to changes in distance ($R$), with a dependance of $R^{-6}$.[20] Using an appropriate fluorescence donor and acceptor pair, FRET may be used as a molecular ruler, with sensitivities of sub-angstrom resolution within the working range of a FRET pair, centered about the Förster distance ($R_0$), or distance of half-maximal energy transfer.[21] FRET has been utilized for probing inter- and intramolecular interactions of proteins in vitro and in vivo. However, since environmental factors, such as solvent exposure and composition, can have large effects on $E_{FRET}$, many factors must be controlled for and monitored, such as the donor quantum yield ($\phi$), acceptor molar extinction coefficient ($\varepsilon$), and overlap of donor emission and acceptor excitation spectra.[17,22]

Acridon-2-ylalanine (Acd, $\delta$) is an intrinsically fluorescent, small (222 Å$^3$, only 45% larger than tryptophan) and uncharged noncanonical amino acid (ncAA) with a high $\phi$ in aqueous media (0.95), a long fluorescence lifetime (8–14 ns), and high photostability (**Figure 2**).[23–25] Additionally, Acd may be incorporated site specifically into a protein of interest using amber stop codon suppression with a cognate tRNA/tRNA synthetase pair orthogonal to an expression host's native translation machinery, also termed genetic code expansion (GCE).[23,24,26,27] With excitation maxima at 385/400 nm and emission maxima at 420/450 nm, Acd may act as both a donor for common longer-wavelength chromophores, including fluorophores such as boron dipyrromethene (BODIPY, Bdp) and

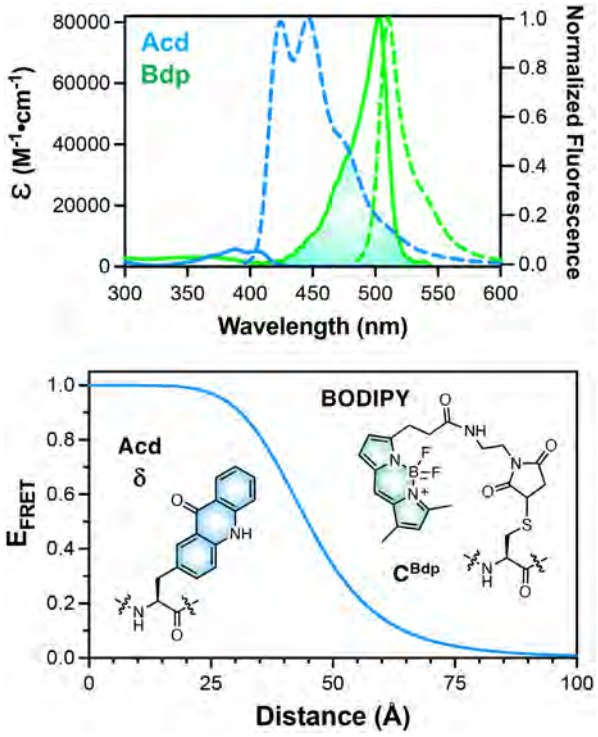


**Figure 2.** Acd and BODIPY spectra, structures, and FRET distance dependance. Top: Acd (blue) and BODIPY (green) absorption (solid lines) and emission (dashed lines) spectra, with spectral overlap region shaded. Absorption spectra are scaled according to $\varepsilon$ at their absorption maximum (left *y*-axis). Emission spectra are normalized to their emission maximum (right *y*-axis). Bottom: Distance dependance of $E_{FRET}$ for Acd and BODIPY based on spectral data and $\phi = 0.95$. Acd and BODIPY structures shown with BODIPY in the form of a $C^{BDP}$ conjugate.

quenchers like copper 1,4,7,10-tetraazacyclododecane, as well as an acceptor for shorter-wavelength fluorescent molecules such as tryptophan and methoxycoumarin.[17,24,28–32] BODIPY is a particularly good FRET acceptor for Acd since it has a narrower excitation peak than similar fluorophores like fluorescein, giving it a lower extinction coefficient in the 400 nm region where Acd is excited, thereby minimizing direct excitation in doubly labeled FRET constructs (Figure 2).[17]

We desired to use Acd/Bdp FRET to observe potential conformational shifts in αS fibrils upon addition of ligands developed as radiotracer leads for PD and MSA PET imaging probes. Photocrosslinking and mass spectrometry (XL-MS, **Figure 3**A) indicate that the lead molecule BF-2846 binds in the well-folded αS fibril core, and autoradiography in patient tissue shows that BF-2846 is nonselective for PD versus MSA. In contrast, M503 and HY-215 bind selectively to PD and MSA patient tissue, respectively, and XL-MS indicates that HY-215 interacts with a region in the αS C-terminus.[11,12] Thus, we wished to understand differences in interactions with this region among these three structurally related ligands, which might help to explain their selectivity profiles. To do this, we generated several fluorescently labeled αS constructs, formed fibrils in mixtures with wild-type (WT) αS, and measured fluorescence spectra to track any conformational changes induced by ligand binding.

## 2. Results and Discussion

### 2.1. Binding Site Identification

Our development of PET ligands for PD and MSA began with the identification of potential ligand binding pockets observed in the original ssNMR structure of αS fibrils (Protein data bank ID (PDB ID): 2n0a).[8,33] Several binding sites were hypothesized in this study, shown in Figure 3. Site 2 is located near residues Y39-E46 in the ssNMR structure, and site 9 is located near residues G86-K96. These sites presented deeper binding pockets than site 3 (K43-H50), site 7 (V63-G67), or site 8 (T81-E83), the only other sites that were surface accessible and in the ordered regions of the fibril. For purposes of clarification, ex vivo fibrils refer to structures isolated directly from patient tissues, whereas in vitro fibrils refers to structures generated in a laboratory setting which may or may not have been seeded with fragments of fibrils isolated from patient tissues. More recent cryo-EM structural data (exemplified by PDB ID: 6h6b) shows that in vitro αS fibrils commonly exist as multiprotofilament structures and that this can result in a rearrangement of site 2 and site 3 (backbone rotation that places Y39 and H50 on the same face of the protofilament) to form a site that we will refer to as site 2* (Figure 1).[34] Indeed, recent studies on the binding of site 2* ligands indicate that the conditions used for our fibril preparation in our studies generate fibrils with a 6h6b-like morphology (PDB ID: 904b),[35] but with a more ordered N-terminus, similar to that recently reported by Jiang et al. (PDB ID: 9c5r).[36] The more ordered N-terminus presents site 1 (G14-T22), as a potential ligand-binding location. The 6h6b, 904b, and 9c5r structures bear substantial similarity to ex vivo structures of fibrils from MSA patients (exemplified by PDB ID: 6xyo),[3] particularly at the level of the conformation within a single fibril strand, with varied strand–strand packing (Figure 1). Both the in vitro and ex vivo MSA structures differ significantly from the ex vivo structure of fibrils from PD patients (Figure 1)[4] as well as the structure of in vitro fibrils formed by seeding with material from Lewy body dementia patients.[5] Thus, we interpret our ligand binding and XL-MS data with in vitro fibrils primarily in terms of the 9c5r structure, since this recapitulates many features of other in vitro αS fibril folds, but resolves portions of the C-terminus relevant to the current study. We note that site 8 is blocked by this positioning of the C-terminus and is not fully available in either the PD or MSA ex vivo structures, so it will not be discussed further.

In Figure 3, XL-MS data for the three ligands are mapped onto the in vitro ssNMR and cryo-EM structures, and the highest-confidence data for selective ligands are mapped onto the PD ex vivo structure (M503) and the MSA structure (HY-215). Initial XL-MS with αS fibrils using an azide derivative of BF-2846 and matrix-assisted laser desorption ionization MS (MALDI-MS) identified site 9 as the primary binding site,[15] and subsequent XL-MS using a diazirine CLX derivative and electrospray ionization MS (ESI-MS) identified other binding sites near site 2 and site 3 (Figure 3B and ESI, Figure S1–S2, Supporting Information). These XL-MS sites are consistent with BF-2846 binding being largely, but imperfectly, orthogonal to compounds that bind to

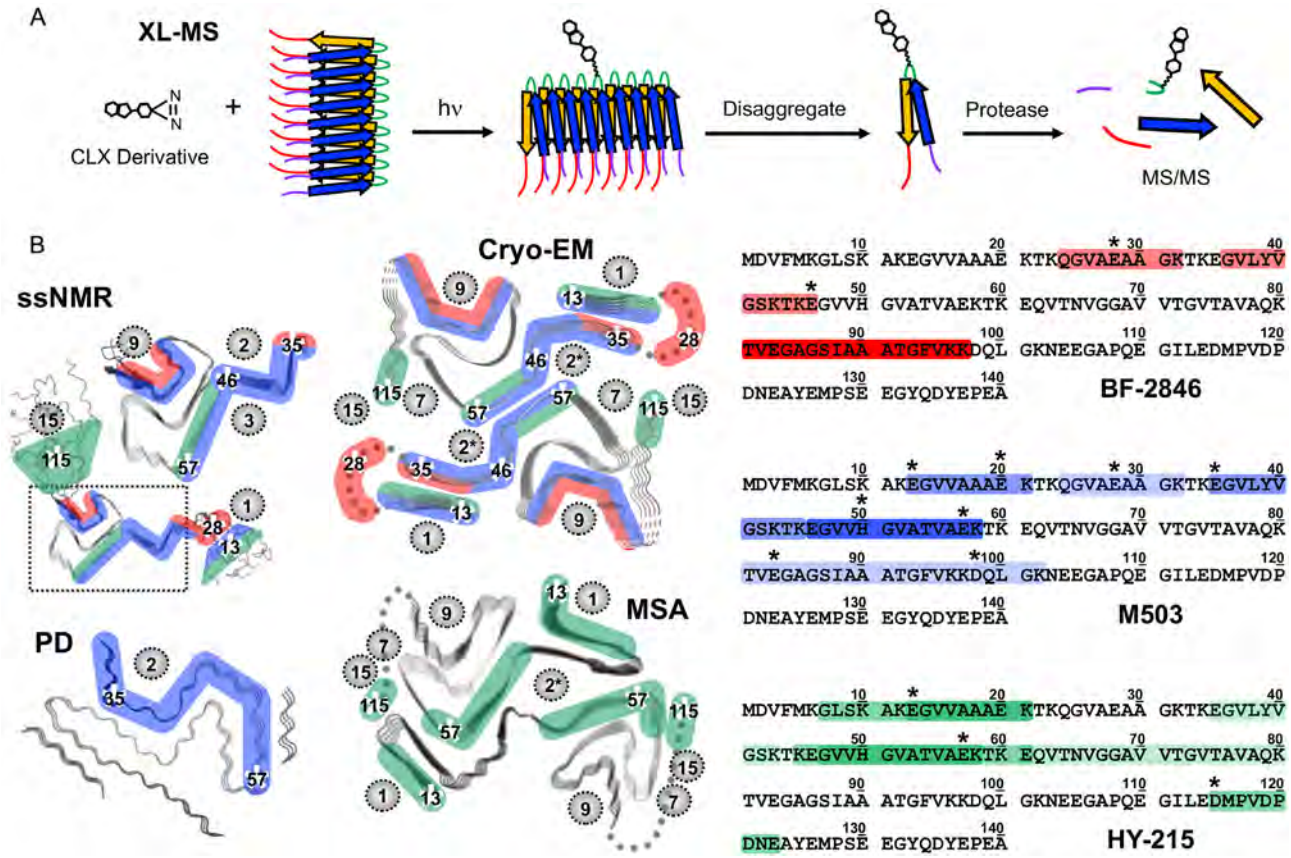


**Figure 3.** Photo-crosslinking sites mapped onto αS sequence and fibril structures. A) XL-MS workflow. B) Crosslink mapping: For both sequences and structures, regions corresponding to peptides observed in XL-MS experiments are highlighted in red (BF-2846), blue (M503), or green (HY-215), with asterisks showing the specific crosslinked residues identified by MS2 fragmentation. For the structures (shown in the same orientations as in Figure 1), binding sites identified in an initial computational screen are identified with gray spheres. For the sequences, the intensity of shading indicates the confidence in XL-MS assignment, based on spectra counts, multiple overlapping peaks identified, or identification of the same site with multiple probes. XL-MS experiments were performed on in vitro fibrils, and all XL-MS data are shown on the ssNMR and cryo-EM structures. Only the highest confidence M503 sites are shown on the PD structure, and only the highest confidence HY-215 sites are shown on the MSA structure. Some HY-215 and BF-2846 XL-MS data have been published previously.[12,15]

site 2*, such as Tg-190b.[33] HY-215 has also been synthesized with a CLX tag (Figure 1), and XL-MS identified binding to site 1, site 2*, site 7, and site 15 (D115-E123), a region that had not been previously observed for XL-MS of any other ligands (Figure 3B). Although this was predicted as a weak binding site in early computational studies,[33] it was not seriously considered since this region has been disordered in almost all cryo-EM and ssNMR structures reported to date.[6] However, in the 9cr5 structure it packs against site 7, creating a binding pocket.[36] M503 binding has not been previously studied by XL-MS, so we prepared a CLX derivative (Figure 1) and photo-crosslinked it to fibrils prepared using our typical aggregation conditions. Following disaggregation to αS monomers and digestion with trypsin (cleaves at Lys and Arg residues) or GluC (cleaves at Asp and Glu residues), we identified crosslinked peptides using MALDI-MS. Collisional MS/MS fragmentation was used to determine the specific residues with M503 crosslinks (Figure S3, Supporting Information). From these data, we see that M503 binds to sites 1, 2*, and 9 (Figure 3B). Thus, it seems that replacing the piperazine group in BF-2846 with a 3.8-diazabicyclo [3.2.1]octane in HY-215 reduced site 9 binding and generated new site 1 and site 15 interactions. In contrast, replacement of the aniline ring of BF-2846 with a carboxypyrimidine bearing an exocyclic amine in M503 favors site 2 binding and does not generate interactions with sites 7 and 15. Given the overall similarity of these ligands and the unusual site 15 interaction of HY-215, we were interested in determining whether conformational changes in the C-terminus played a role in binding for any of the three ligands.

### 2.2. Protein Design, Expression, and Labeling

FRET studies require production of doubly labeled protein, and proper interpretation of distance information also requires production of donor-only and acceptor-only control proteins. We used the available structural information to choose label sites for our αS constructs that would effectively report on conformational changes and minimize any disruptive effects of the fluorescent probes. The residues we chose to mutate were Ser9, Phe94, Glu114, and Tyr125, placing a FRET donor in the N-terminus to be paired with a FRET acceptor at site 9 (94), or on either side of site

15 (114 and 125). These sites have previously shown to be non-perturbative to mutation in previous fluorescent labeling studies.[18,37] Based on the 2n0a (ssNMR) and 9c5r (cryo-EM) structures, we were able to estimate the distances between pairs of these residues, with separations of 9/94: 45 Å, 9/114: 65 Å, and 9/125: >40 Å. Since the 125 position is not fully resolved in any available structure, we were only able to estimate a lower bound for the 9/125 distance. This information allowed us to choose a FRET donor/acceptor pair with an appropriate working distance range. We have previously labeled αS with cyanophenylalanine/Trp, cyanophenylalanine/ thioamide, Trp/Acd, Acd/methoxycoumarin, fluorescein/rhodamine FRET pairs, as well AlexaFluor, or Atto dyes for single-molecule FRET studies.[17,18,28,37–42] Here, we chose Acd/Bdp, because the $R_0$ of about 42 Å for this pair gives a working range of 30–65 Å (10%–90% $E_{FRET}$) that is well-matched to the expected residue-to-residue distance ranges. Additionally, Acd/Bdp double labeled constructs can be fairly easily produced through Acd incorporation by GCE and labeling of a Cys residue with BODIPY maleimide (Bdp-Mal) to produce $C^{Bdp}$ (Figure 2);[17] the visible wavelength nature of these probes reduces artifacts due to light scattering experienced with UV probes like Trp;[43] and the smaller size of Acd makes it less likely to disrupt protein interactions than fluorescein and rhodamine.[44] Taken together, these characteristics make Acd/Bdp an ideal, minimalist FRET pair for studying changes in αS fibril structure.

Double-labeled constructs, along with the corresponding Acd-only or Bdp-only single-labeled control constructs, were created by inserting TAG and/or TGC codons for respective amber suppression and cysteine insertion in the pTXB1-αS expression plasmid. The pTXB1 plasmid includes a C-terminal intein and $His_6$ tag, which is convenient to eliminate protein truncation that may occur due to incomplete suppression of the stop codon.[45] These plasmids were then transformed into BL21-DE3 *E. coli* cells for expression, along with a pDule2 plasmid containing sequences for the Acd aminoacyl tRNA synthetase (RS) and cognate tRNA pair, derived from a *Methanocaldococcus jannaschii* RS/tRNA pair (**Figure 4**).[26] Protein constructs were expressed and purified using Ni-agarose resin, fast protein liquid chromatography (FPLC), and high performance liquid chromatography (HPLC). Mutant cysteine containing constructs were labeled with Bdp-Mal and purified once again by HPLC. Final protein yields for Acd-only constructs were about 50% of WT αS, and yields for Bdp-labeled constructs were about 25% of WT αS (Table S1, Supporting Information). Final labeled protein purity was confirmed by MALDI-MS (Figure S4–S5, Supporting Information). Calculated versus observed masses may be found in Table S1, Supporting Information.

### 2.3. Fibril FRET Studies

Labeled proteins were mixed in a ratio of 95:5 with WT αS, and aggregated at 100 μM total protein concentrations in monomer units in phosphate buffered saline (PBS) with 1300 rpm orbital shaking in a 37 °C incubator for 5 days (**Figure 5**). This WT/labeled ratio allows for good fluorescence signal while

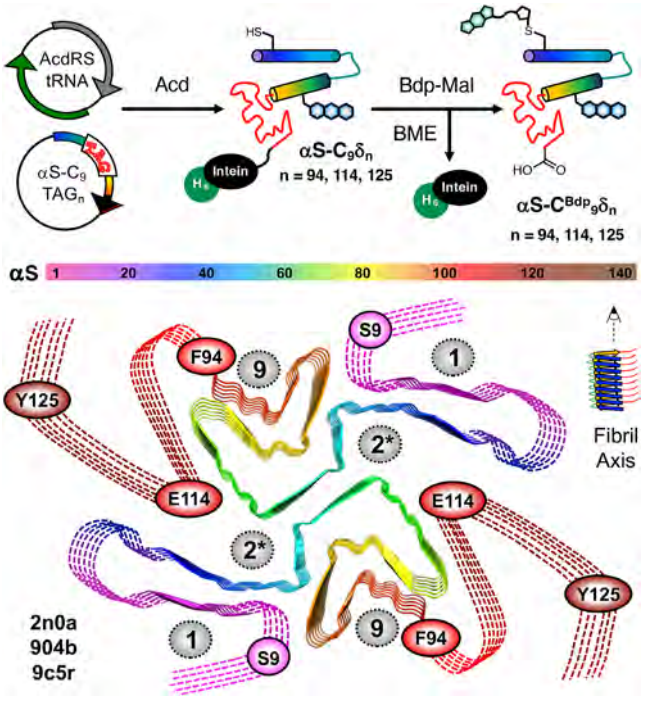


**Figure 4.** αS Acd/Bdp construct expression and labeling strategy. Top: *Escherichia coli* (*E.coli*) cells are transformed with a plasmid for the AcdRS/tRNA pair and a plasmid for the protein (αS) with a Cys mutation at the site of BODIPY labeling and a TAG codon at the site of Acd labeling. The protein is expressed as a $His_6$-tagged intein fusion, purified, labeled with Bdp-Mal, the intein cleaved, and the protein further purified to give the Acd/Bdp double-labeled protein (αS-$C^{BDP}{}_9\delta_n$, $n = 94, 114, 125$) for FRET studies. Bottom: Model of fluorophore placement (colored ovals) and binding sites (gray spheres) on in vitro αS fibrils based on 904b and 9c5r cryo-EM structures and 2n0a ssNMR structure.[8,35,36]

maintaining native fibril structure and minimizing intermolecular FRET interactions, which would confound interpretation of intramolecular distance changes.[46] The aggregated constructs were then diluted and their emission spectra from 430 to 600 nm were acquired, with excitation at 410 nm. In previous FRET studies with this pair in αS, this wavelength was found to sufficiently excite the donor fluorophore with minimal direct Bdp excitation.[17] Direct excitation of the Bdp in double-labeled and Bdp-only fibrils at 490 nm was also used to determine whether any quenching of the acceptor occurred. The fibril solutions were then treated with BF-2846, M503, or HY-215 and allowed to incubate, with shaking, for 4 or 24 h. The emission spectra were acquired again using the same excitation and emission wavelengths. All experiments were performed in triplicate and averaged. A spectrum of 100% WT αS taken under identical compound treatment conditions was used for background correction of all spectra.

Before performing more in-depth analysis, we normalized the spectra for the double-labeled constructs to determine whether any change in FRET was apparent in the presence of the compounds (**Figure 6**). No change in the ratio of Acd emission at 445 nm to Bdp emission at 510 nm is observed in the dimethyl sulfoxide (DMSO) treated fibrils for any of the three donor–acceptor combinations. This indicates that there are

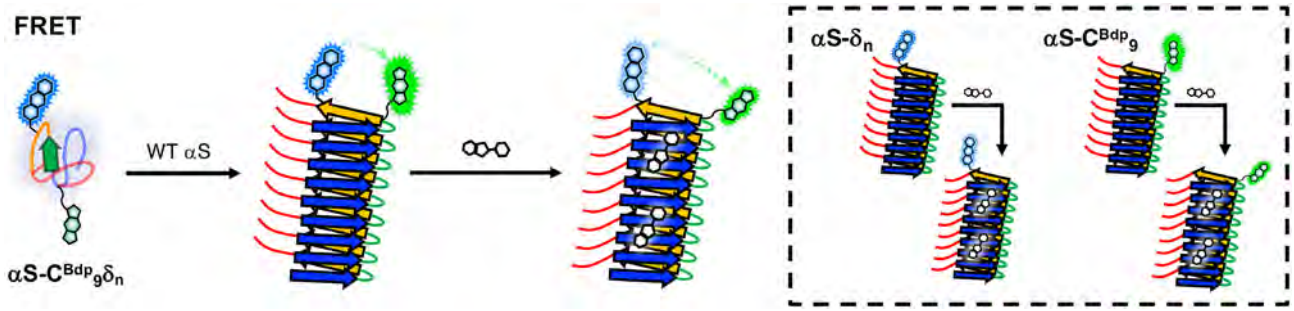


**Figure 5.** αS fibril FRET. Experimental scheme for making fibrils with 5% αS-C$^{Bdp}_9$δ$_n$, $n = 94$, 114, or 125 (double-labeled) and treating them with BF-2846, M503, or HY-215. Inset: Control experiments with fibrils made from 5% αS-δ$_n$, $n = 94$, 114, or 125 (donor-only) or 5% αS-C$^{Bdp}_9$ (acceptor-only).

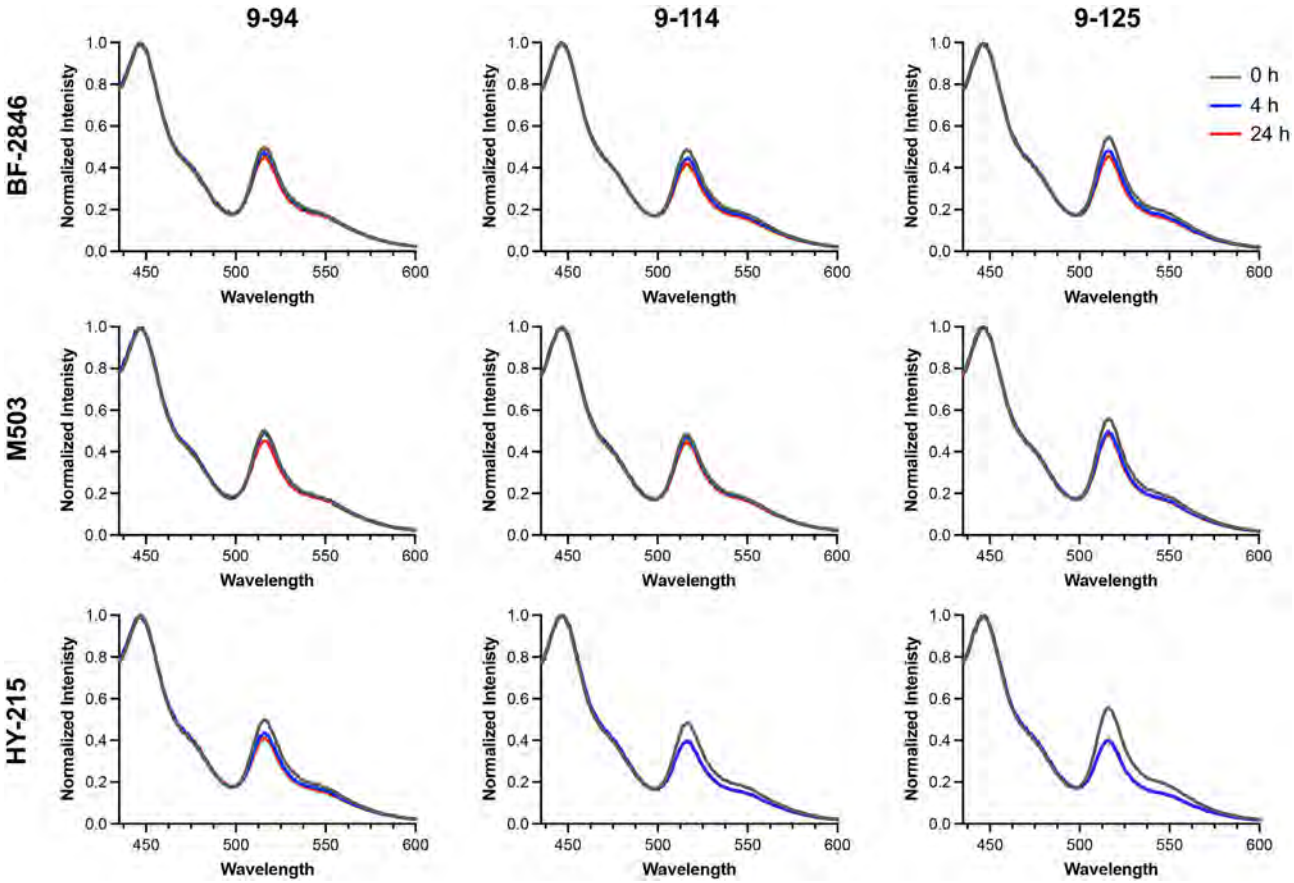


**Figure 6.** Normalized spectra for αS Acd/Bdp fibrils. Changes in the relative intensity of the Bdp peak at 510 nm reflect changes in FRET efficiency resulting from changes to chromophore environments and interchromophore distances.

no background conformational changes upon DMSO addition, consistent with our previous studies.[17] In examining the Acd/Bdp ratios in the compound-treated fibrils, several things are clear immediately. HY-215 has the most significant effect on the fibrils, decreasing the Acd/Bdp ratio for all three FRET pairs, with a particularly strong effect on 9–125. BF-2846 and M503 have almost no effect on 9–94 of 9–114, and a smaller effect than HY-215 on 9–125. Finally, in all cases, the 4 and 24 h spectra are nearly identical, implying that the conformational changes take place shortly after compound addition. These observations are consistent with the XL-MS data that show crosslinking to the C-terminus only for HY-215.

We then used nonnormalized data to perform a more in-depth analysis of HY-215 induced conformational changes. As shown in **Figure 7**, there is overall quenching of fluorescence upon addition of HY-215 to the labeled fibrils. Similar effects were observed with BF-2846 and M503, but not the DMSO vehicle (Figure S6–S17, Supporting Information). Thus, changes in FRET must be interpreted carefully using donor-only and acceptor-only controls. For example, for the 9–94 FRET pair

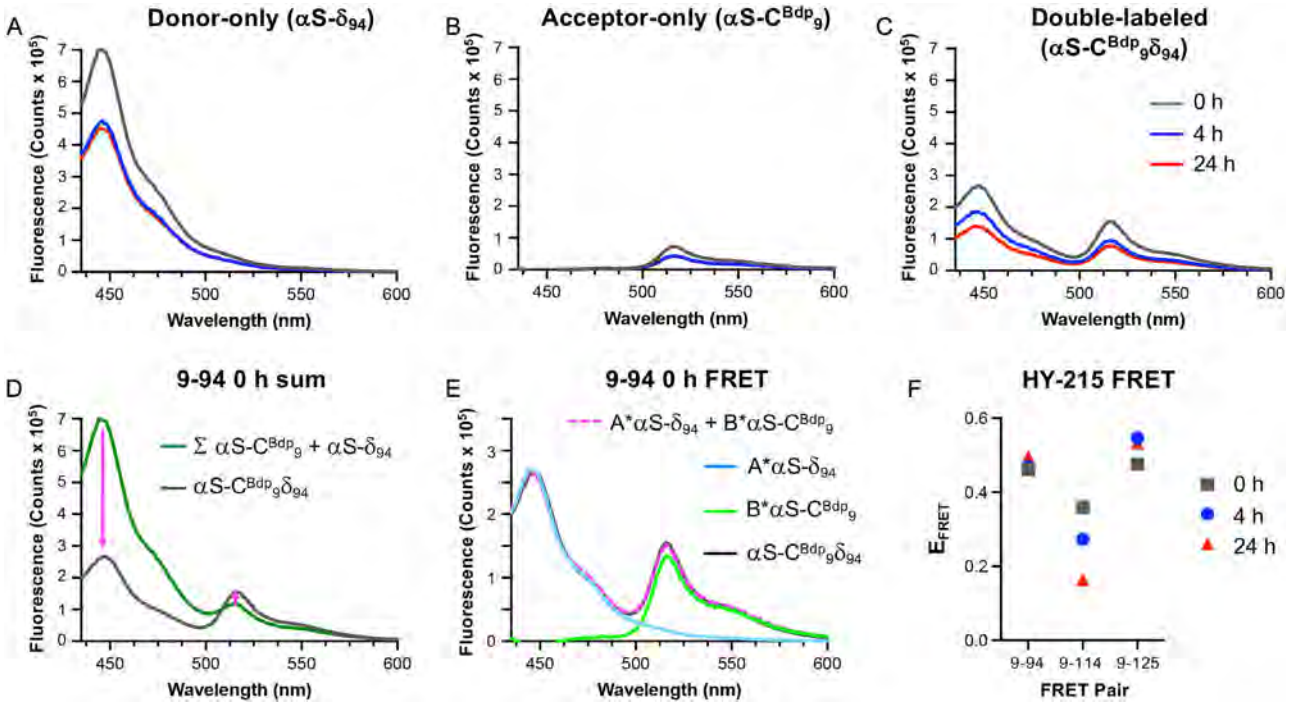


**Figure 7.** αS fibril FRET. Top: Raw spectra for untreated fibrils (0 h) and fibrils treated for 4 or 24 h with HY-215; A) donor-only controls, B) acceptor-only controls, C) double-labeled fibrils. Bottom: D) FRET analysis of untreated fibrils showing a comparison of the double-labeled spectrum to the sum of donor-only and acceptor-only spectra, E) an example $E_{FRET}$ calculation for untreated fibril data showing the weighted donor-only and acceptor-only spectra as well as their sum compared to the double-labeled spectrum, and F) a chart showing $E_{FRET}$ for each FRET pair for untreated fibrils (0 h) and after 4 or 24 h of HY-215 treatment.

one can see that there are changes in the αS-$\delta_{94}$ and αS-$C^{Bdp}{}_9$ spectra in the presence of HY-215, indicating that there are effects that are independent of FRET. When one compares the sum of the donor-only and acceptor-only spectra to the spectrum of the double-labeled protein, it is clear that there is a decrease in Acd emission and an increase in $C^{Bdp}$ emission, demonstrating a FRET interaction in untreated fibrils (Figure 7D). Although there is an overall decrease in emission intensity for the double-labeled protein (Figure 7C), when one examines the donor-only and acceptor-only spectra (Figure 7A,6B), one can see that the relative intensities are nearly identical, implying that 9–94 FRET is unchanged upon addition of HY-215, consistent with our analysis of the normalized spectra. Donor-only and acceptor-only spectra are also essential to FRET-based calculations of distance changes.

To determine $E_{FRET}$, we fit the αS-$C^{Bdp}{}_9\delta_n$ doubly labeled spectrum to a linear combination of the singly labeled spectra by adjusting the A and B parameters in this equation to minimize the square difference

$$\sum_{\lambda}(I(\lambda)_{DA} - (AI(\lambda)_D + BI(\lambda)_A))^2 \quad (1)$$

where $I(\lambda)_{DA}$, $I(\lambda)_D$, and $I(\lambda)_A$ represent the fluorescence intensity at a given wavelength from double-labeled αS-$C^{Bdp}{}_9\delta_n$, donor-only αS-$\delta_n$, and acceptor-only αS-$C^{Bdp}{}_9$, respectively (Figure 7E, Figure S15–S17, Supporting Information). From this fit, $E_{FRET}$ is then calculated as

$$E_{FRET} = \left[S_A * (1 - A) + S_B * \left(\frac{\varepsilon_A}{\varepsilon_D}\right)(B - 1)\right] \quad (2)$$

where $\varepsilon_A/\varepsilon_D$ is the ratio of the acceptor and donor extinction coefficients at the excitation wavelength (410 nm) and the weighting factors of $S_A$ and $S_B$ reflect the relative contributions of the donor-only and acceptor-only spectra. For untreated fibrils (t = 0 h), we obtain $E_{FRET}$ values of 0.42 ± 0.02, 0.38 ± 0.04, and 0.45 ± 0.01 for 9–94, 9–114, and 9–125 FRET pairs, respectively. The small standard deviations show that we are able to make consistent measurements across the different fibril samples, as seen in the agreement between t = 0 h values for the fibrils to be treated with BF-2846, M503, or HY-215, which should all be identical prior to compound addition (Table S2, Supporting Information). Using the same approach, we determined $E_{FRET}$ for all three FRET pairs after 4 or 24 h treatments with HY-215 (Figure 7F). There is essentially no change for the 9–94 FRET pair, and a very minor change for 9–125, but a significant decrease in $E_{FRET}$ for 9–114.

To properly estimate interchromophore distance from $E_{FRET}$, we must determine $R_0$ for Acd and $C^{Bdp}$ in this environment by comparing the emissions of the Acd-only construct and free Acd amino acid to calculate the donor quantum yield $\phi_D$ in the fibril in the presence of the compound. We find that Acd is quenched significantly, with $\phi_D$ decreasing from 0.95 for the free amino acid in water to 0.69 at position 94, 0.79 at position 114, and 0.71 at position 125 in untreated fibrils (Table S3, Supporting Information). A fully rigorous determination of $R_0$ would also

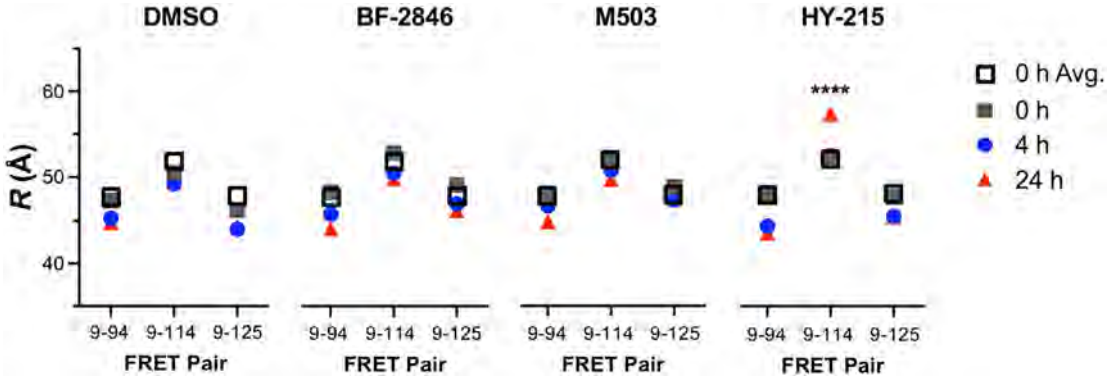


**Figure 8.** Distance changes in fibrils. *R* for each FRET pair for untreated fibrils and after 4 or 24 h of compound or DMSO treatment. Expansion is observed for 9–94 under HY-215 treatment. Compaction is observed for all other FRET conditions, including DMSO treatment. Open squares indicate the average distances for all untreated samples. *R* values given in Table S6, Supporting Information. Only the HY-215 9–114 distance change at 24 h is statistically significant relative to both untreated fibril measurements and DMSO-treated fibril measurements (both $p < 0.0001$, ****). Full analysis of the statistical significance of distance measurements is given in Table S7, S8, Supporting Information.

require determining the acceptor extinction coefficient, $\varepsilon_A$, and the spectral overlap integral, *J*, in the fibril environment. However, these values do not typically change with environment as much as $\phi_D$ and can be difficult to measure for dilute samples. Using the $\phi_D$ correction, we determine an $R_0$ value of 44.7 ± 0.6 Å for 9–94 in untreated fibrils, from which we calculate a distance, *R*, of 47.2 ± 0.2 Å. This result is in reasonable agreement with the $C_\alpha$–$C_\beta$ distance for $Gly_{14}$ (the last resolved N-terminal residue in the 9c5r structure) and $Phe_{94}$ of 44 Å.

By performing the same fitting procedure for the fibril spectra in the presence of the compounds, we can determine $E_{FRET}$ and the corresponding Acd-Bdp distance, *R*, after correcting for changes in $\phi_D$. The 9–94 distance is shortened by 2–4 Å under all treatment conditions, including DMSO vehicle. Thus, it seems that there is not a significant change in the fibril core upon compound binding, consistent with most cryo-EM structures of fibrils with compounds bound that have been reported to date.[13,14,35] While one might be concerned that compound binding to site 9 would affect FRET measurements, since only 1-in-20 αS molecules has Acd at position 94, the vast majority of the binding sites are unperturbed. Distance data for all FRET pairs and conditions are summarized in **Figure 8** and Table S6, Supporting Information. Experimental error of <2 Å is estimated based on the variance among the three replicate spectra which were averaged for each donor-only, acceptor-only and double-labeled spectrum used in the calculations (Figure S18 and Table S2, Supporting Information). This can also be seen by comparison of the average distance for each FRET pair across all samples to the distance calculated for each condition at t = 0 h (Figure 8). Since these are all untreated fibrils, the distances should be identical.

In contrast to 9–94, differences in effects between the three compounds are seen for Acd label sites in the C-terminus. For 9–114 FRET pairs, a slight compaction is seen for BF-2846 or M503 after 4 or 24 h of treatment, with a more significant expansion from 53 Å to 59 Å for HY-215 after 24 h. For 9–125 FRET pairs, small compactions are seen for all three ligands. In general, these changes are consistent with the interpretation from simple inspection of the normalized spectra for the double-labeled constructs (Figure 6). However, it is notable that the apparent decrease FRET seen for the 9–125 pairs in the normalized spectra becomes a negligible change in interchromophore distance when one corrects for effects of the donor-only or acceptor-only control spectra. This is particularly significant for HY-215 data, where binding in the C-terminus appears to quench Acd fluorescence, necessitating corrections for the donor spectra and $\phi_D$ (see Table S3–S5, Supporting Information). Additional investigations of these binding phenomena would be advisable using nonphotometric methods such as calorimetry, surface plasmon resonance, NMR, or electron paramagnetic resonance with spin-tagged probes.

Taken together, these experiments show that unlike the nonselective parent compound BF-2846 or the PD-selective compound M503, HY-215 binds to the region around Asp115 (site 15) and induces a conformational change in that region. While there are differences in strand–strand packing between the in vitro fibril structures (e.g. PDB ID 9c5r) and the MSA fibril structures, there is similarity in the site 7 region and presumably in the way that the C-terminus packs against it (Figure 3) that could be exploited to design MSA-specific compounds.

## 3. Conclusion

Our findings provide further insight into the differential binding of these PET imaging probe candidates. While the primary binding sites of all three ligands are expected to be in the well-folded fibril core, the different interactions with the C-terminus that we have observed may play an important role in their selectivity. In particular, for HY-215, transient folding of the region around Asp115 may allow it to bind, followed by a conformational change to form a more stable binding pocket. However, one must keep in mind that these experiments were done on in vitro fibrils. While these are expected to have substantial similarity to MSA fibrils, particularly at the level of the fold in an individual strand, the structures of in vitro fibrils are not identical to the ex vivo MSA

fibril structures (Figure 1). Additionally, since ex vivo PD fibrils structures are significantly differently than MSA or in vitro fibril structures, M503 may interact quite differently with PD fibrils, in spite of the tempting interpretation that its interactions with site 2 confer PD-selectivity. Another factor that may complicate relating these effects to fibrils in vivo is posttranslational modification, particularly phosphorylation of Ser129 ($pS_{129}$), the most common modification of αS, and one often used as a biomarker for pathological αS.[47,48] To investigate compound binding to PD fibril polymorphs, we can use methods for templating aggregation using patient material which have been shown to successfully replicate the fold of αS from Lewy bodies (i.e. PD).[5] In fact, we have previously used PD and MSA patient material seeding methods in which we incorporated fluorescently labeled protein in the templated fibrils for cell uptake studies.[49] Moreover, we have shown that we can synthesize or express αS with a variety of posttranslational modifications, including $pS_{129}$, and that these can be combined with fluorescent labeling.[40,50,51] Thus, we can investigate the effects of modifications like $pS_{129}$ on binding of HY-215 and M503, and this can even be done in the context of fibrils templated with PD patient material.

## 4. Experimental Section

### Construction of pTXB1-αS–$S_9$C, $F_{94}$TAG, $E_{114}$TAG, and $Y_{125}$TAG Plasmids

Site directed mutagenesis was performed on three previously constructed pTXB1_αSyn-Mxe-$His_6$ mutants, $F_{94}$TAG, $E_{114}$TAG, and $Y_{125}$TAG. Quikchange polymerase chain reaction using Q5 Hotstart High-Fidelity DNA Polymerase was performed on each TAG containing mutant to generate the double mutants, and once on the wild-type αSyn to generate the single $S_9$C mutation, all bearing a polyhistidine-tagged GyrA intein from *Mycobacterium xenopi* (Mxe) fuzed to the C-terminus of the αSyn to aid in purification.

### αS-WT and αS-$C_9$ Expression

αS mutant plasmids (pTXB1_αS-WT-Mxe-$His_6$ or pTXB1_αS-$C_9$-Mxe-$His_6$) were transformed into competent *E. coli* BL21(DE3) cells and plated onto LB agar plates supplemented with ampicillin (Amp) overnight at 37 °C. Single colonies were used to inoculate 5 mL of LB media supplemented with Amp (100 μg $mL^{-1}$). Primary cultures were incubated at 37 °C with shaking at 250 rpm overnight. A single primary culture was used to inoculate L of LB media supplemented with AMP (100 μg $mL^{-1}$) and grown at 37 °C and shaking at 250 rpm until $OD_{600}$ was measured between 0.6 and 0.9. Expression was then induced with IPTG (1 mM) and then placed at 18 °C with shaking at 250 rpm overnight.

### αS-$\delta_{94}$, αS-$\delta_{114}$, αS-$\delta_{125}$, αS-$C_9\delta_{94}$, αS-$C_9\delta_{114}$, and αS-$C_9\delta_{125}$ Expression

αS mutant plasmids (pTXB1_αS-$TAG_{94}$-Mxe-$His_6$, pTXB1_αS-$TAG_{114}$-Mxe-$His_6$, pTXB1_αS-$TAG_{125}$-Mxe-$His_6$, pTXB1_αS-$C_9TAG_{94}$-Mxe-$His_6$, pTXB1_αS-$C_9TAG_{114}$-Mxe-$His_6$, or pTXB1_αS-$C_9TAG_{125}$-Mxe-$His_6$) and an AcdRS/tRNA plasmid (pDule2_MjAcdRSA9) were transformed into competent *E. coli* BL21(DE3) cells and plated onto LB agar plates supplemented with Amp and streptomycin (Strep), overnight at 37 °C. Single colonies were selected and used to inoculate 5 mL of LB supplemented with Amp and Strep (100 μg $mL^{-1}$ of each) and left to shake at 250 rpm and 37 °C overnight. Single primary cultures were used to inoculate 1 L of M9 media (100 mL 10x M9 salts, 2 mM $MgSO_4$, 15 μg $mL^{-1}$ $FeCl_2$, 15 μg $mL^{-1}$ $ZnCl_2$, 10 nM $CaCl_2$, 0.02% yeast extract, 0.5% glucose) supplemented with Amp and Strep at 37 °C and shaking at 250 rpm until $OD_{600}$ was between 0.6 and 0.9. At this time, Acd amino acid was added (0.5 mM) and culture was allowed to incubate for five more minutes. Expression was then induced by adding IPTG (1 mM) and the culture was placed at 18 °C shaking at 250 rpm overnight.

### Purification of αS Constructs

Cells were harvested by centrifugation at 4,000 rpm in a GS3 rotor and Sorvall RC-5 centrifuge for 20 min at 4 °C. The supernatant was discarded and the cell pellet was resuspended in 20 mL of resuspension buffer (40 mM Tris, pH 8.3) containing PMSF (0.1 mM) and two Roche protease inhibitor cocktail pills (cOmplete, Mini, EDTA-free protease inhibitor cocktail, glass vial, Roche cat. #11836170001). Resuspended cells were then lysed by sonication on ice (Amp: 30, process time: 5 min, pulse on: 1 sec, pulse off: 2 sec) and then pelleted at 14,000 rpm in a Sorvall RC-5 centrifuge with an SS-34 rotor for 20 min at 4 °C. The supernatant was collected and incubated with $Ni^{2+}$-NTA resin (5 mL column volume) for 1 h at 4 °C with rotation. The slurry was then added to a fritted column and the liquid allowed to flow through. The resin was then washed with 2 × 13 mL of wash buffer A (50 mM HEPES, pH 7.5) and 2 × 13 mL of wash buffer B (50 mM HEPES, 5 mM imidazole, pH 7.5). The protein constructs were eluted from the resin with 2 × 6 mL of elution buffer (50 mM HEPES, 300 mM imidazole, pH 7.5). The elution fractions were then pooled and treated with β-mercaptoethanol (βME, 200 mM) for intein cleavage at RT for 18 h on a rotisserie. The resulting cleavage solution was then dialyzed against 20 mM Tris pH 8.0 overnight. The dialyzed solution was then reapplied to 5 mL of $Ni^{2+}$-NTA and allowed to incubate at 4 °C with rotation for 1 h. The slurry was then applied to a fritted column and allowed to flow through. The resin was washed once with 13 mL of wash buffer A and pooled with previously collected flow-through and dialyzed against a 20 mM Tris, pH 8.0 buffer at 4 °C overnight. Prior to FPLC purification, all Cys containing constructs were treated with TCEP Bond-Breaker (1 mM) to reduce any disulfides formed between αS proteins and/or βME. Each construct was purified by ion exchange chromatography using a HiTrap Q HP column (5 mL) on an ÄKTA FPLC using a 65 min NaCl gradient (0 to 450 mM NaCl in 20 mM Tris, pH 8.0). The fractions containing pure product were identified using MALDI-MS. The αS Cys containing mutant constructs were dialyzed against a 20 mM Tris, pH 8.0 buffer at 4 °C overnight. αS-WT and αS-$\delta_{Acd}$ containing mutant constructs were dialyzed against 1 x PBS buffer (137 mM NaCl, 2.7 mM KCl, 10 mM $Na_2HPO_4$, 1.8 mM $KH_2PO_4$, pH 7.4) at 4 °C and further purified via HPLC with a protein C4 column (Phenomenex Jupiter #00G-4168-N0) with pure fractions being identified by MALDI-MS. Pure protein fractions were pooled and dialyzed against 1x PBS buffer at 4 °C overnight. Following dialysis, proteins were concentrated via centrifugation with a 3 kDa cutoff filter, stored at −80 °C in 1 mL aliquots, and thawed once for experiments. The Cys containing mutants were immediately subject to labeling following purification.

### αS Labeling with Bdp-FL-Mal

The Cys containing protein solutions following post-FPLC purification dialysis (ca. 10–20 mL) were separated into 5 mL aliquots and treated with TCEP Bond-Breaker (1 mM). To each protein solution was added 50 mM Bdp-Mal in DMSO to a final concentration of 200 μM in dye. The labeling reaction was allowed to proceed for 3 h on a rotisserie at RT. Each step was monitored by MALDI-MS. After labeling was deemed complete, each solution was dialyzed against a 20 mM Tris, pH 8.0 buffer at 4 °C for 4 h to remove extreme excess of dye. The dialyzed solution was concentrated via centrifugation with a 3 kDa cutoff filter (Cytiva # 28,932,358). The concentrated solution was then additionally purified via HPLC with a protein C4 column (Phenomenex Jupiter #00G-4168-N0) and pure protein fractions were identified via MALDI-MS. Pure protein fractions were pooled and dialyzed against 1 x PBS buffer at 4 °C overnight. Following dialysis, proteins were concentrated via centrifugation with a 3 kDa cutoff filter, stored at −80 °C in 1 mL aliquots, and thawed once for experiments.

### αS FRET Measurements: Fibril Preparation

Protein construct concentrations were determined by detergent compatible assay analysis. αS monomer was combined to a final concentration of 100 μM and 95:5 unlabeled to labeled construct in 1x PBS. Each aliquot was treated with sodium azide to a final concentration of 0.2% to restrict bacterial growth. The tubes were sealed with Teflon and Parafilm and incubated at 37 °C with shaking at 1300 rpm for 3–5 days. The fibrils were then pelleted and the supernatant removed to get rid of any unincorporated monomer. Pellets were then reconstituted in fresh 1x PBS with 0.2% sodium azide.

### αS FRET Measurements: FRET Measurements

αS fibrils were diluted to a final concentration of 10 μM (relative to αS monomer) into 1x PBS buffer and pipetted in triplicate into nonsterile Greiner black, flat μClear, 96 well half area microplates (#675096) to a final volume of 100 μL. Additionally, Bdp dye, Acd amino acid, αS-$C^{Bdp}_9$, αS-$\delta_{94}$, αS-$\delta_{114}$, αS-$\delta_{125}$, αS-$C^{Bdp}_9\delta_{114}$, and αS-$C^{Bdp}_9\delta_{125}$ monomer were all diluted to 0.5 μM and subject to the same conditions as below to act as controls and as comparison for data analysis. Prior to small molecule addition, fluorescence intensity values were obtained for each construct to optimize gain and Z-position using $\lambda_{ex} = 385 \pm 5$ nm and reading at $\lambda_{em} = 420 \pm 5$ nm since Acd is expected to have the highest fluorescence intensity. Additionally, fluorescence intensity was measured exciting at $490 \pm 5$ nm and reading at $515 \pm 5$ nm to optimize gain and Z-position for direct Bdp excitation. T0h emission scans were obtained for each construct prior to small molecule addition using the parameters previously acquired and optimized, exciting at $\lambda_{ex} = 410 \pm 5$ nm, scanning from $\lambda_{em} = 425$ to $600 \pm 5$ nm, in 1 nm increments, and a 40 μs integration time. Direct excitation of Bdp was also acquired at $\lambda_{ex} = 490 \pm 5$ nm and measuring from $\lambda_{em} = 505$ to $600 \pm 5$ nm using the same step size and integration time as previously mentioned. Small molecule was then added in triplicate to a final concentration of 10 μM. The plates were then covered with an anti-evaporation guard and placed at 37 °C with shaking at 500 rpm. Measurements were taken using the same parameters at 4 h and 24 h post-small molecule addition. Spectra for al constructs and data fitting to determine FRET parameters are described in Supporting Information.

## Supporting Information

Additional mass spectrometry and fluorescence data as well as descriptions of chemical synthesis and mass spectrometry procedures. The authors have cited additional references within the Supporting Information.[11,12,17,18,24,52–54]

## Acknowledgements

This work was supported in part by the University of Pennsylvania and the National Institutes of Health (NIH RF1 NS103873 to E.J.P., U19 NS110456 to E.J.P. and R.H.M., and R01 HD106051 to B.A.G.). R.M.P. thanks the NIH for funding through the Chemistry Biology Interface Training Program (T32 GM133398) and an Individual Predoctoral Fellowship (F31 AG090063). M.G.L. was supported by an Age Related Neurodegenerative Disease Training Grant fellowship (NIH T32 AG000255). Instruments supported by the NIH and NSF include NMR (NSF CHE 1827457) and mass spectrometers (NIH S10 OD030460).

## Conflicts of Interest

The authors declare no conflict of interest.

## Data Availability Statement

The data that support the findings of this study are available from the corresponding author upon reasonable request.

**Keywords:** alpha-synuclein · fluorescence · noncanonical amino acids · Parkinson's disease · photo-crosslinking

[1] S. Koga, H. Sekiya, N. Kondru, O. A. Ross, D. W. Dickson, *Mol. Neurodegener.* **2021**, *16*, 83.
[2] K. A. Jellinger, *Parkinsonism Relat. Disord.* **2023**, *107*, 105273.
[3] M. Schweighauser, Y. Shi, A. Tarutani, F. Kametani, A. G. Murzin, B. Ghetti, T. Matsubara, T. Tomita, T. Ando, K. Hasegawa, S. Murayama, M. Yoshida, M. Hasegawa, S. H. W. Scheres, M. Goedert, *Nature* **2020**, *585*, 464.
[4] Y. Yang, Y. Shi, M. Schweighauser, X. Zhang, A. Kotecha, A. G. Murzin, H. J. Garringer, P. W. Cullinane, Y. Saito, T. Foroud, T. T. Warner, K. Hasegawa, R. Vidal, S. Murayama, T. Revesz, B. Ghetti, M. Hasegawa, T. Lashley, S. H. W. Scheres, M. Goedert, *Nature* **2022**, *610*, 791.
[5] D. D. Dhavale, A. M. Barclay, C. G. Borcik, K. Basore, D. A. Berthold, I. R. Gordon, J. Liu, M. H. Milchberg, J. Y. O'Shea, M. J. Rau, Z. Smith, S. Sen, B. Summers, J. Smith, O. A. Warmuth, R. J. Perrin, J. S. Perlmutter, Q. Chen, J. A. J. Fitzpatrick, C. D. Schwieters, E. Tajkhorshid, C. M. Rienstra, P. T. Kotzbauer, *Nat. Commun.* **2024**, *15*, 2750.
[6] M. H. Milchberg, O. A. Warmuth, C. G. Borcik, D. D. Dhavale, E. R. Wright, P. T. Kotzbauer, C. M. Rienstra, *Biophys. J.* **2025**, *124*, 2571.
[7] C.-L. Chen, M.-C. Kuo, W.-C. Wu, Y.-C. Hsu, R.-M. Wu, W.-Y. I. Tseng, *NeuroImage: Clin.* **2022**, *34*, 102997.
[8] M. D. Tuttle, G. Comellas, A. J. Nieuwkoop, D. J. Covell, D. A. Berthold, K. D. Kloepper, J. M. Courtney, J. K. Kim, A. M. Barclay, A. Kendall, W. Wan, G. Stubbs, C. D. Schwieters, V. M. Y. Lee, J. M. George, C. M. Rienstra, *Nat. Struct. Mol. Biol.* **2016**, *23*, 409.
[9] J. Therriault, S. E. Schindler, G. Salvadó, T. A. Pascoal, A. L. Benedet, N. J. Ashton, T. K. Karikari, L. Apostolova, M. E. Murray, I. Verberk, J. W. Vogel, R. La Joie, S. Gauthier, C. Teunissen, G. D. Rabinovici,

H. Zetterberg, R. J. Bateman, P. Scheltens, K. Blennow, R. Sperling, O. Hansson, C. R. Jack, P. Rosa-Neto, *Nat. Rev. Neurol.* **2024**, *20*, 232.
[10] M. M. Alam, S. H. Lee, S. Wasim, S.-Y. Lee, *Arch. Pharm. Res.* **2025**, *48*, 333.
[11] G.-L. Tian, C.-J. Hsieh, D. S. Guarino, T. J. A. Graham, Z. Lengyel-Zhand, A. Schmitz, W. K. Chia, A. J. Young, J.-G. Crosby, K. Plakas, T. Huang, H. Jiang, Y. Yu, C. Hou, H. Lee, E. J. Petersson, S. Giannakoulias, J. O'Shea, P. Kotzbauer, Z. Tu, C. A. Mathis, R. H. Mach, *Rsc Med. Chem.* **2025**, *16*, 2743.
[12] H. Y. Kim, W. K. Chia, C.-J. Hsieh, D. S. Guarino, T. J. A. Graham, Z. Lengyel-Zhand, M. Schneider, C. Tomita, M. G. Lougee, H. J. Kim, V. V. Pagar, H. Lee, C. Hou, B. A. Garcia, E. J. Petersson, J. O'Shea, P. T. Kotzbauer, C. A. Mathis, V. M. Y. Lee, K. C. Luk, R. H. Mach, *J. Med. Chem.* **2023**, *66*, 12185.
[13] Y. Tao, W. Xia, Q. Zhao, H. Xiang, C. Han, S. Zhang, W. Gu, W. Tang, Y. Li, L. Tan, D. Li, C. Liu, *Nat. Chem. Biol.* **2023**, *19*, 1235.
[14] J. Xiang, Y. Tao, Y. Xia, S. Luo, Q. Zhao, B. Li, X. Zhang, Y. Sun, W. Xia, M. Zhang, S. S. Kang, E.-H. Ahn, X. Liu, F. Xie, Y. Guan, J. J. Yang, L. Bu, S. Wu, X. Wang, X. Cao, C. Liu, Z. Zhang, D. Li, K. Ye, *Cell* **2023**, *186*, 3.
[15] J. J. Ferrie, Z. Lengyel-Zhand, B. Janssen, M. G. Lougee, S. Giannakoulias, C. J. Hsieh, V. V. Pagar, C. C. Weng, H. Xu, T. J. A. Graham, V. M. Lee, R. H. Mach, E. J. Petersson, *Chem. Sci.* **2020**, *11*, 12746.
[16] M. G. Lougee, V. V. Pagar, H. J. Kim, S. X. Pancoe, W. K. Chia, R. H. Mach, B. A. Garcia, E. J. Petersson, *Chem. Commun.* **2022**, *58*, 9116.
[17] M. B. Cory, C. M. Jones, K. D. Shaffer, Y. Venkatesh, S. Giannakoulias, R. M. Perez, M. G. Lougee, E. Hummingbird, V. V. Pagar, C. M. Hurley, A. Li, R. H. Mach, R. M. Kohli, E. J. Petersson, *Protein Sci.* **2023**, *32*, e4633.
[18] J. J. Ferrie, C. M. Haney, J. Yoon, B. Pan, Y.-C. Lin, Z. Fakhraai, E. Rhoades, A. Nath, E. J. Petersson, *Biophys. J.* **2018**, *114*, 53.
[19] B. W. Van Der Meer, G. Coker Ill, S.-Y. S. Chen, *Resonance Energy Transfer*, VCH Publishers, Inc, New York, NY U.S.A **1994**.
[20] L. Stryer, R. P. Haugland, *Proc. Natl. Acad. Sci. U. S. A.* **1967**, *58*, 719–726.
[21] J. Lakowicz, *Principles of Fluorescence Spectroscopy*, Springer, New York **2006**, *1*.
[22] D. B. VanBeek, M. C. Zwier, J. M. Shorb, B. P. Krueger, *Biophys. J.* **2007**, *92*, 4168.
[23] C. M. Jones, D. M. Robkis, R. J. Blizzard, M. Munari, Y. Venkatesh, T. S. Mihaila, A. J. Eddins, R. A. Mehl, W. N. Zagotta, S. E. Gordon, E. J. Petersson, *Chem. Sci.* **2021**, *12*, 11955.
[24] L. C. Speight, A. K. Muthusamy, J. M. Goldberg, J. B. Warner, R. F. Wissner, T. S. Willi, B. F. Woodman, R. A. Mehl, E. J. Petersson, *J. Am. Chem. Soc.* **2013**, *135*, 18806.
[25] A. Szymanska, K. Wegner, L. Lankiewicz, *Helv. Chim. Acta* **2003**, *86*, 3326.
[26] I. Sungwienwong, Z. M. Hostetler, R. J. Blizzard, J. J. Porter, C. M. Driggers, L. Z. Mbengi, J. A. Villegas, L. C. Speight, J. G. Saven, J. J. Perona, R. M. Kohli, R. A. Mehl, E. J. Petersson, *Org. Biomol. Chem.* **2017**, *15*, 3603.
[27] S. Avila-Crump, M. L. Hemshorn, C. M. Jones, L. Mbengi, K. Meyer, J. A. Griffis, S. Jana, G. E. Petrina, V. V. Pagar, P. A. Karplus, E. J. Petersson, J. J. Perona, R. A. Mehl, R. B. Cooley, *ACS Chem. Biol.* **2022**, *17*, 3458.
[28] J. J. Ferrie, N. Ieda, C. M. Haney, C. R. Walters, I. Sungwienwong, J. Yoon, E. J. Petersson, *Chem Commun* **2017**, *53*, 11072.
[29] C. M. Jones, Y. Venkatesh, E. J. Petersson, in *Methods in Enzymology*, (Eds: D. M. Chenoweth), Academic Press, Cambridge, MA **2020**, *639*, 37–69.
[30] W. N. Zagotta, B. S. Sim, A. K. Nhim, M. M. Raza, E. G. Evans, Y. Venkatesh, C. M. Jones, R. A. Mehl, E. J. Petersson, S. E. Gordon, *Elife* **2021**, *10*, e70236.
[31] S. E. Gordon, E. G. B. Evans, S. C. Otto, M. H. Tessmer, K. D. Shaffer, M. T. Gordon, E. J. Petersson, S. Stoll, W. N. Zagotta, *Biophys. J.* **2024**, *123*, 2063.
[32] W. N. Zagotta, E. G. B. Evans, P. Eggan, M. H. Tessmer, K. D. Shaffer, E. J. Petersson, S. Stoll, S. E. Gordon, *Biophys. J.* **2024**, *123*, 2050.
[33] C.-J. Hsieh, J. J. Ferrie, K. Xu, I. Lee, T. J. A. Graham, Z. Tu, J. Yu, D. Dhavale, P. Kotzbauer, E. J. Petersson, R. H. Mach, *Acs Chem. Neurosci.* **2018**, *9*, 2521.
[34] R. Guerrero-Ferreira, N. M. I. Taylor, D. Mona, P. Ringler, M. E. Lauer, R. Riek, M. Britschgi, H. Stahlberg, *ELife* **2018**, *7*, e36404.
[35] J. C. Sanchez, R. M. Perez, D. S. Guarino, D. Dhavala, J. K. Baumgardt, K. D. Shaffer, P. Kotzbauer, R. H. Mach, E. J. Petersson, E. R. Wright, *BioRxiv* **2025**, 2025.2006 2030 662461.
[36] C. Sun, K. Zhou, P. I. V. DePaola, C. Li, V. M. Y. Lee, Z. H. Zhou, C. Peng, L. Jiang, *J. Biol. Chem.*, **2025**, *301*, 108351.
[37] C. M. Haney, C. L. Cleveland, R. F. Wissner, L. Owei, J. Robustelli, M. J. Daniels, M. Canyurt, P. Rodriguez, H. Ischiropoulos, T. Baumgart, E. J. Petersson, *Biochemistry* **2017**, *56*, 683.
[38] C. M. Haney, R. F. Wissner, J. B. Warner, Y. J. Wang, J. J. Ferrie, D. J. Covell, R. J. Karpowicz, V. M. Y. Lee, E. J. Petersson, *Org. Biomol. Chem.* **2016**, *14*, 1584.
[39] T. Tanaka, A. M. Wagner, J. B. Warner, Y. J. Wang, E. J. Petersson, *Angew. Chem., Int. Ed.*, **2013**, *52*, 6210.
[40] B. Pan, E. Rhoades, E. J. Petersson, *ACS Chem. Biol.* **2020**, *15*, 640.
[41] S. Batjargal, Y. J. Wang, J. M. Goldberg, R. F. Wissner, E. J. Petersson, *J. Am. Chem. Soc.* **2012**, *134*, 9172.
[42] R. F. Wissner, S. Batjargal, C. M. Fadzen, E. J. Petersson, *J. Am. Chem. Soc.* **2013**, *135*, 6529.
[43] C. M. Haney, R. F. Wissner, E. J. Petersson, *Curr. Opin. Chem. Biol.* **2015**, *28*, 123.
[44] L. C. Speight, M. Samanta, E. J. Petersson, *Aust. J. Chem.* **2014**, *67*, 686.
[45] S. Batjargal, C. R. Walters, E. J. Petersson, *J. Am. Chem. Soc.* **2015**, *137*, 1734.
[46] C. M. Haney, E. J. Petersson, *Chem. Commun.* **2018**, *54*, 833.
[47] C. H. Gibbons, T. Levine, C. Adler, B. Bellaire, N. Wang, J. Stohl, P. Agarwal, G. M. Aldridge, A. Barboi, V. G. H. Evidente, D. Galasko, M. D. Geschwind, A. Gonzalez-Duarte, R. Gil, M. Gudesblatt, S. H. Isaacson, H. Kaufmann, P. Khemani, R. Kumar, G. Lamotte, A. J. Liu, N. R. McFarland, M. Miglis, A. Reynolds, G. A. Sahagian, M.-H. Saint-Hillaire, J. B. Schwartzbard, W. Singer, M. J. Soileau, S. Vernino, , et al., *JAMA* **2024**, *331*, 1298.
[48] S. X. Pancoe, Y. J. Wang, M. Shimogawa, R. M. Perez, S. Giannakoulias, E. J. Petersson, *J. Mol. Biol.* **2022**, *434*, 167859.
[49] N. P. Marotta, J. Ara, N. Uemura, M. G. Lougee, E. S. Meymand, B. Zhang, E. J. Petersson, J. Q. Trojanowski, V. M. Y. Lee, *Acta Neuropathol. Commun.* **2021**, *9*, 188.
[50] B. Pan, N. Kamo, M. Shimogawa, Y. Huang, A. Kashina, E. Rhoades, E. J. Petersson, *J. Am. Chem. Soc.* **2020**, *142*, 21786.
[51] I. G. Saleh, M. Shimogawa, J. Ramirez, B. Abakah, Y. Venkatesh, H. P. James, M.-H. Li, S. A. Louie, M. G. Lougee, W.-K. Chia, R. B. Cooley, R. A. Mehl, T. Baumgart, R. H. Mach, D. Eliezer, E. Rhoades, E. J. Petersson, *Protein Sci.* **2025**, *34*, e70302.
[52] Y. Fukuyama, R. Tanimura, K. Maeda, M. Watanabe, S.-I. Kawabata, S. Iwamoto, S. Izumi, K. Tanaka, *Anal. Chem.* **2012**, *84*, 4237.
[53] J. G. Marmorstein, V. V. Pagar, E. Hummingbird, I. G. Saleh, H. A. T. Phan, Y. Chang, K. D. Shaffer, Y. Venkatesh, I. J. Dmochowski, K. J. Stebe, E. J. Petersson, *Bioconjug. Chem.* **2024**, *35*, 1913.
[54] M. Puchades, A. Westman, K. Blennow, P. Davidsson, *Rapid Commun. Mass Spectrom.*, **1999**, *13*, 344.

Manuscript received: July 31, 2025
Revised manuscript received: September 27, 2025
Version of record online: October 13, 2025